High flux polysulfone braided hollow fiber membrane for wastewater treatment role of zinc oxide as hydrophilic enhancer

Peechmani, Prakash; Othman, Mohd Hafiz Dzarfan; Kamaludin, Roziana; Puteh, Mohd Hafiz; Jaafar, Juhana; Rahman, Mukhlis A; Ismail, Ahmad Fauzi; Kadir, Siti Hamimah Sheikh Abdul; Illias, Rosli Md.; Gallagher, Joe; Djuli, Sabreenna Marsya

Published in:
Journal of Environmental Chemical Engineering

DOI:
10.1016/j.jece.2021.105873

Publication date:
2021

Citation for published version (APA):
Peechmani, P., Othman, M. H. D., Kamaludin, R., Puteh, M. H., Jaafar, J., Rahman, M. A., Ismail, A. F., Kadir, S. H. S. A., Illias, R. M., Gallagher, J., & Djuli, S. M. (2021). High flux polysulfone braided hollow fiber membrane for wastewater treatment role of zinc oxide as hydrophilic enhancer. *Journal of Environmental Chemical Engineering*, *9*(5), [105873]. https://doi.org/10.1016/j.jece.2021.105873

High Flux Polysulfone Braided Hollow Fiber Membrane for Wastewater Treatment Role of Zinc Oxide as Hydrophilic Enhancer

Prakash Peechmani[1], Mohd Hafiz Dzarfan Othman[1*], Roziana Kamaludin[1,] Mohd Hafiz Puteh[1,2], Juhana Jaafar[1], Mukhlis A Rahman[1], Ahmad Fauzi Ismail[1], Siti Hamimah Sheikh Abdul Kadir[3], Rosli Md. Illias[4], Joe Gallagher[5], Sabreenna Marsya Djuli[3]

[1]*Advanced Membrane Technology Research Centre (AMTEC), Universiti Teknologi Malaysia, 81310 Skudai, Johor.*

[2]*Department of Environmental Engineering, School of Civil Engineering, Universiti Teknologi Malaysia, 81310 Skudai, Johor.*

[3] *Institute of Pathology, Laboratory and Forensic Medicine (I-PPerForM), Universiti Teknologi Mara (UiTM), Cawangan Selangor, Kampus Sungai Buloh, Jalan Hospital 47000 Sungai Buloh, Malaysia*

[4]*Department of Bioprocess and Polymer Engineering, School of Chemical and Energy Engineering, Universiti Teknologi Malaysia, 81310 Skudai, Johor.*

[5]*Institute of Biological, Environmental & Rural Sciences (IBERS), Aberystwyth University, Gogerddan, Aberystwyth, Ceredigion, SY23 3EE United Kingdom.*

**Corresponding author: hafiz@petroleum.utm.my*

Abstract

Incorporation of zinc oxide (ZnO) nanoparticles has played an important role on the improvement of unique membrane characterization and performance, most notably the hydrophilic modification of the membrane for higher pure water permeability. Additionally, the permeability of the membrane can be improved via introduction of braid support by reducing the thickness of the membrane separation layer. Moreover, the braided hollow fiber membrane (BHFM) is able to perform under higher pressure conditions compared to hollow fiber membranes. In this paper, hybrid polysulfone (PSf)/ZnO BHFMs were fabricated via phase inversion method. Hydrophilic 10 ± 1.8nm polycrystalline ZnO nanoparticles synthesized via sol-gel method were incorporated on BHFM to improve the hydrophilicity and increase flux with constant rejection under high pressure and the effect of the ZnO loading on the membrane properties and performance were

thoroughly studied. The fabricated BHFMs with 0.0, 0.5, 1.0 and 1.5 wt.% of ZnO nanoparticles concentration were defined as BHFM1, BHFM2, BHFM3 and BHFM4 respectively. Scanning electron microscopy (SEM), contact angle, mechanical strength, flux performance, rejection with bovine serum albumin (BSA) and fouling of best performed membrane were conducted to achieve the target of this paper. The performance of these hybrid ZnO/PSf BHFMs were compared with neat PSf hollow fiber membrane (HFM) and previous studies. The findings from this research work shows that BHFM4 has the most desired properties for wastewater treatment application. The ZnO nanoparticles in BHFM4 have improved hydrophilicity from 108.79 to 71.02°, and thus BHFM4 has increased flux performance from 36.20 to 919.12 L/m^{2}h at 1.0 bar pressure and 193.48 to 1909.11 L/m^{2}h at 4.0 bar pressure when compared with BHFM1. Constant BSA rejection rates (>90%) were observed in all BHFMs. The improved hydrophilicity and pure flux performance with constant rejection rate in high pressure conditions illustrates the suitability of fabricated ZnO/PSf BHFMs in wastewater treatment applications.

Keywords:

Braided hollow fiber membrane; Zinc oxide; Polysulfone; Water treatment; High flux

1.0 Introduction

The performance of membrane material plays an important role in the membrane application, operational condition, operational cost and effluent quality of the wastewater treatment system [1–3]. The high molecular weight of PSf makes this polymer suitable for use in membrane filtrations particularly for water [4,5], pharmaceutical [6], textile dyeing [7,8], desalination [9], peat water [10] and sewage wastewater[11] treatment systems. The excellent mechanical strength, its stability at pH levels from 2 to 13, excellent resistance to caustic and good resistance to moderate chlorine are qualities of PSf which make it suitable to be used for membrane filtration even though it is hydrophobic in nature [5,11–16]. In detail, the excellent mechanical strength ensures the membranes are able to operate at higher pressure, the capability of PSf which can withstand from low to high pH range allows the filtration process to operate at high temperature [6] and the good tolerance to moderate chlorine makes it very suitable for use in any water and wastewater filtration system. However, the hydrophobic nature of PSf membranes

means that the flux obtained from the filtration is low. Therefore, PSf membranes need some surface modification to enhance the permeation of water molecules.

From the literature study, high flux rate of the PSf membrane can be improved via incorporation of hydrophilic nanoparticles [4]. Some examples of nanoparticles are titanium dioxide (TiO_2) nanomaterials, ZnO nanoparticles, silver (Ag) nanoparticles, carbon nanotubes (CNTs), and graphene oxide (GO) [17–19]. Among them, ZnO nanoparticles are considered to be a promising metal oxide for PSf membrane modification due to its high hydrophilicity, relatively inexpensive cost and is non-toxic to humans [20,21]. The hydrophilic nature of the ZnO nanoparticles can easily absorb hydroxyl (-OH) groups which increases the absorption of water molecules onto the separation layer of membrane [22]. This water-loving characteristic of ZnO nanoparticles is able to increase the overall flux performance of membranes. Antifouling of organic matters by hydrophilic ZnO nanoparticles also adds value for the incorporation of these nanoparticles in mixed matrix membranes. Organic matters are less susceptible to foul on the hydrophilic membranes due to the reduced interactions between the hydrophilic membrane surface with organic matters [23]. Xiong et al. reported ZnO nanoparticles are able to improve hydrophilicity and porosity of the nanocomposite substrate membranes [24]. Amini et al. [25] reported that the contact angle values observed were lower as the ZnO nanoparticles loading increased. Moreover, with increasing amount of ZnO nanoparticles in the membrane matrix, the reverse salt flux of thin film nanocomposite (TFN) membranes also increased. This can be related to the soluble permeability or hydrophilicity of the membrane. Kusworo et al.[26] found that 1.5 wt% of ZnO nanoparticle increased the hydrophilic property of PES membrane from 68.33˚ to 66.17˚. They explained that it's due to the nature of a higher volume of nano-ZnO particles which have a large surface area on the membrane that can adsorb hydrophilic -OH and therefore increases the hydrophilicity. Sokhandan et al. [27] reported introduction of hydrophilic agents such as 2.0 wt.% of sodium alginate ($C_6H_7O_6Na$) in 2 wt.% ZnO improved the flux from 37 to 51 L/m^2h, porosity from 63.00 to 72.00%, antibacterial nature, higher flux recovery from 33.50 to 74.00% and hydrophilicity from 42.00 to 28.00° for sodium alginate coated zinc oxide in Polyacrylonitrile (ZnO@SA/PAN) flat sheet membrane.

Apart from the hydrophilic surface modification, a few studies have successfully reported that the introduction of braid support in membrane fabrication has increased flux performance of microfiltration and ultrafiltration membranes by reducing the thickness of the separation layer and its reliability in high pressure conditions compared to hollow fiber membranes [28–31]. From literature, it was also reported that the braid support in hollow fiber membranes is able to improve the overall mechanical strength and can ensure the longer lifetime of the membranes [32–34]. The good flux performance and excellent mechanical strength of BHFMs make them suitable for high pressure submerged filtration systems. Two spinning methods were reported to fabricate defect-free BHFMs, namely non-solvent induced phase inversion (NIPS) [35] and electrospinning [36]. Between these two methods, membranes fabricated via NIPS methods are giving more flux due to their thin separation layers. From the literature, incorporation of the ZnO nanoparticles in braided hollow fiber membranes have not been studied. Hence, this current research aims to prepare high flux PSf BHFMs by incorporating hydrophilic ZnO nanoparticles in hydrophobic PSf BHFMs via NIPS method. The presence of ZnO nanoparticles can be beneficial in absorbing more water molecules into the braided hollow fiber membranes during the filtration process. This valuable attribute makes the ZnO a promising material to be used in membrane surface modification. Polymeric dope solution with 16 wt.% of PSf and 0.0, 0.5, 1.0 and 1.5 wt.% of ZnO nanoparticles were prepared for the fabrication of BHFMs through NIPS and characterized.

2.0 Materials and methods

2.1 Materials

All chemicals used in this work were of analytical reagent grade unless otherwise stated. Commercial 1.3 mm outer diameter of polyester (PET) braid support was purchased from Philos (South Korea). PSf was purchased from Solvay Specialty Polymer (UDEL® P-3500 LCD MB7). N,N-Dimethylacetamide (DMAc) as solvent was purchased from QReC Chemicals. Zinc acetate ($Zn(CH_3CO_2)_2$), oxalic acid ($C_2H_2O_4$), ethanol (C_2H_5OH) and BSA were purchased from Sigma-Aldrich.

2.2 Synthesis of ZnO nanoparticles

ZnO nanoparticles were synthesized by a previously reported sol-gel method [37,38]. 0.1 M zinc acetate and 0.1 M oxalic acid mixtures (*Zn* $(CH_3CO_2)_2$ / $C_2H_2O_4$) were prepared with gentle stirring in ethanol for 30 min at 60 ± 5 °C and 50 ± 5 °C respectively. The oxalic acid solution was added dropwise to the zinc acetate solution at 60 ± 5 °C. The mixture was then left under vigorous magnetic stirring for 90 min to allow for complete reaction in order to obtain a gel-like zinc oxalate. The operating pH of 2.0 ± 0.2 was obtained by initially adding oxalic acid to the zinc acetate mixture. The resulting gel was then dried at 60 °C overnight in an oven to form the precursors for the ZnO nanoparticles which then underwent calcination at temperatures of 400 °C for 3 h. The chemical reactions of the ZnO synthesis with a suitable temperature for the calcination are summarized as below.

$$\mathbf{Zn(CH_3COO)_2 + H_2C_2O_4 \xrightarrow{60^\circ C} ZnC_2O_4 + 2CH_3COOH} \quad \text{(Equation 1)}$$

$$\mathbf{ZnC_2O_4 \xrightarrow{400^\circ C} ZnO + CO + CO_2 + 2H_2O} \quad \text{(Equation 2)}$$

Equation 1 shows the reaction between the starting materials of zinc acetate and oxalic acid to form the zinc oxalate precursor. Equation 2 shows the precursor undergoing calcination to ensure the removal of impurities and excess carbon monoxide, carbon dioxide and water. Hence, a high purity of ZnO nanoparticles was obtained.

2.3 ZnO/PSf dope preparation

The hybrid ZnO/PSf BHFMs were fabricated through phase inversion method [39]. The compositions of the dope solutions to fabricated ZnO/PSf BHFMs are as shown in Table 1. In short, ZnO nanoparticles were dissolved in DMAc and stirred vigorously for 30 min at 70 °C until homogenous. The obtained solution was then ultrasonicated under ambient conditions for 2 h to promote dispersion of ZnO nanoparticles in the dope solution. Then PSf pallets were added into the ZnO/DMAc mixture and stirred vigorously for 6 h at 70 °C. The prepared dope solution was degassed for 2 h to remove bubbles formed during stirring and stored in the oven at 60 °C for 24

h to remove any residual bubbles. As shown in Table 1, the ZnO/PSf dope solutions were prepared with various ZnO nanoparticles loading concentration, i.e., 0.0, 0.5 , 1.0 and 1.5 wt.%, and labelled as BHFM1, BHFM2, BHFM3 and BHFM4 respectively. Neat PSf HFM was fabricated as a benchmark for the BHFM characterizations.

Table 1 Formulation of dope solution for BHFM fabrication

Membrane code	ZnO nanoparticles (wt.%)	PSf (wt.%)	DMAc (wt.%)
HFM	0.0	16.0	84.0
BHFM1	0.0	16.0	84.0
BHFM2	0.5	16.0	83.5
BHFM3	1.0	16.0	83.0
BHFM4	1.5	16.0	82.5

2.4 Membrane fabrication

The BHFMs were fabricated via phase inversion method using a tube and orifice spinneret with internal diameter of 2.0 mm and outer diameter of 3.0 mm. Prior to the spinning process, the purchased 1.3 mm outer diameter braid support was pretreated with ethanol for 6 h and the braid surface was functionalized by dipping it in 4% NaOH at 80 °C for 2 h [40]. The supports were cleaned three times with deionized water and dried. The pretreated braid support was collected in a winder roller which was fixed at higher elevation than the spinning system and the braid support was guided through from top to bottom of the spinneret system as shown in Figure 1(a). Unlike the typical spinneret system, this BHFM spinneret system does not require any water to form the lumen as the existing braid support already has the lumen, as shown in Figure 1(b). The prepared ZnO/PSf dope solution was transferred into dope reservoir which was then pumped into the spinneret system and extruded out to the coagulation bath tank once the dope is coated on the braid support. The formed membrane was collected in the winding drum as shown in Figure 1(c). This entire coating and phase inversion process was conducted at room temperature (25 ± 2 °C). The air gap distance and take-up speed were set to 10 cm and 2 m/min respectively. After the fabrication of the ZnO/PSf BHFM, the membrane was collected from collecting drum and stored in water (25 °C) for 24 h to remove the residual solvent and water soluble additives from the membrane [28].

(a)

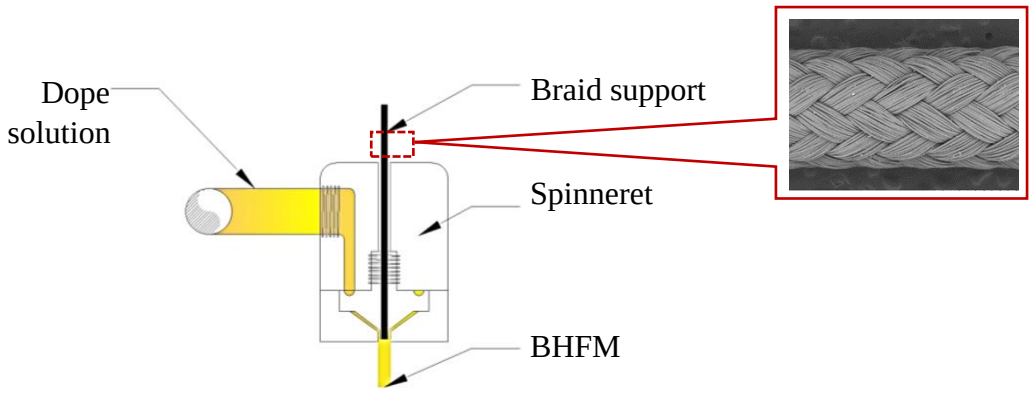

175

(b)

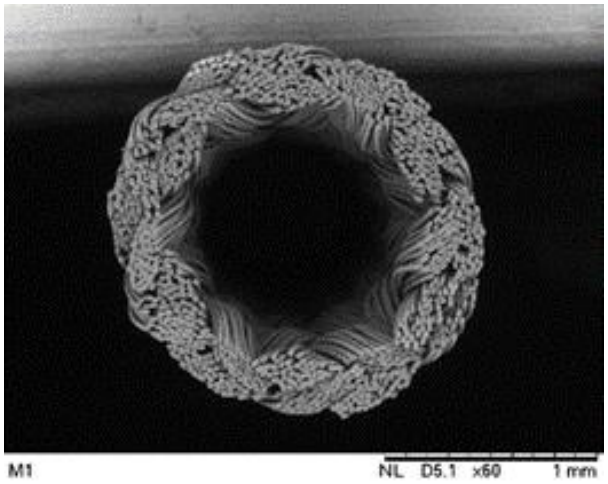

176

177

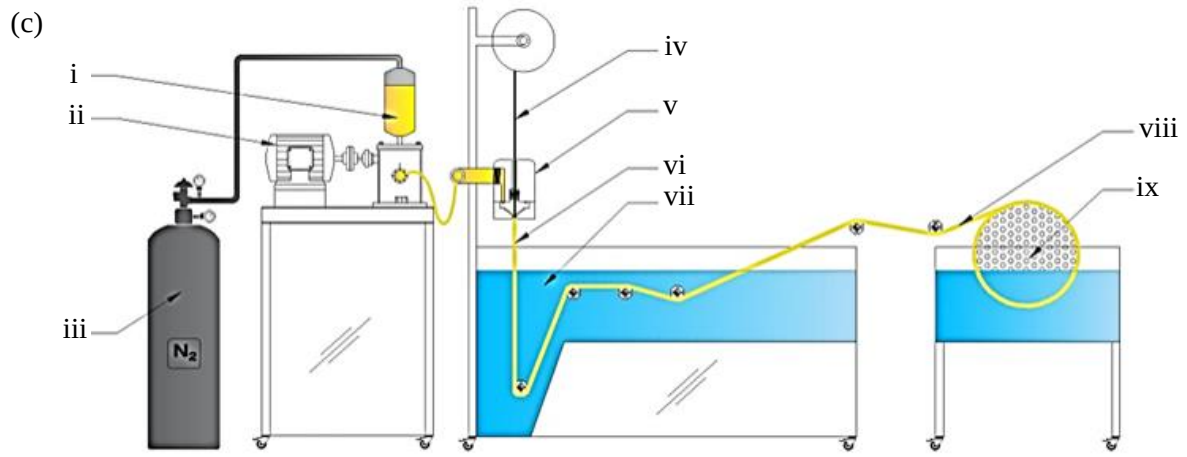

Figure 1 Schematic diagram of the spinning process (a) spinneret, (b) cross-section of PET braid support and (c) Spinning process which consisting of (i) dope solution in reservoir, (ii) gear pump for dope extrusion, (iii) nitrogen gas, (iv) braid support, (v) spinneret, (vi) braid support coated with dope solution, (vii) coagulation bath, (viii) BHFM and (ix) collecting drum.

Meanwhile, self-supported HFM was fabricated via dry-jet wet spinning method using a tube and orifice spinneret with internal diameter of 1.5 mm and outer diameter of 3.0 mm. Reverse osmosis water and tap water were used for internal and external coagulation of the membrane fabrication process respectively. Table 2 shows the spinning parameters that were adopted to fabricate the HFM and BHFMs. The fabricated HFM was immersed in water for 24 h to remove the solvent residue. Both HFM and BHFMs were post-treated with 30 wt.% glycerol solution prior to characterization.

Table 2 Spinning parameters of PSf HFM and BHFMs.

Parameters	**HFM**	**BHFM**
Dope extrusion rate	8.00 mL/min	3.6 mL/min
Air Gap	10 cm	10 cm
Bore fluid rate	15 ml/min	n.a.
Coagulation bath temperature	25 °C	25 °C
Collecting drum speed	12 m/min	2.4 m/min

2.4 Analytical methods

2.4.1 Sample's characterization

X-ray diffraction (XRD) patterns of synthesized ZnO nanoparticles were investigated in 2θ range from 10° to 80° using Bruker diffractometer with Cu_K-beta radiation. The morphologies of the HFM and BHFMs were investigated using Scanning Electron Microscopy (SEM; Model: TM 3000, Hitachi). Prior to the SEM analysis, the HFM was fractured under liquid nitrogen for a clean break, while the BHFMs were cut to clean cross-section by using a surgical scalpel after the BHFMs have been soaked in liquid nitrogen for 5 min. The clean fractured/cut membranes were then sputtered for 5 to 10 min until a thin platinum layer (around 10 nm) coated the surface of the sample to capture high quality cross-sectional images. The SEM images were captured at x60 and x800 magnification. The separating layer thickness of the HFM and BHFMs were measured at 10 selected locations for each cross-section. The outer and inner diameter of the HFM and BHFMs were measured at 3 different randomly selected locations for each cross-section. Surface hydrophilicity was determined via sessile-drop method (Model: OCA 15EC, Dataphysic). The contact angle measurement was taken at 5 randomly selected locations of BHFMs to yield an average result.

2.4.2 Water flux

Water flux experiments were conducted in a membrane module filtration apparatus. For each module, one fibre with 10 cm length was assembled into the filtration module and a pure water flux measurement performed in a cross-flow mode through outside-in configuration. Each membrane sample was tested at 0.5, 1.0, 1.5, 2.0, 3.0, 4.0, 5.0 and 6.0 bar trans-pressure in order to get the permeability of the membranes. Compressed distilled water was used as the permeate for pure water flux measurements. The flux permeation of the membranes was calculated according to Equations 3 and 4:

$$\boldsymbol{F = \frac{V}{Axt}} \qquad \text{(Equation 3)}$$

$$\boldsymbol{A = \pi d_0 L} \qquad \text{(Equation 4)}$$

where F is the membrane flux (L/m^{2}h), V is the volume of permeate at time t (L), A is the effective filtration area of the membrane (m^2), d_o is the outer diameter of hollow fibers (cm) and L is the effective length of hollow fibers (cm).

2.4.3 BSA rejection

Rejection test was conducted in membrane module filtration apparatus using bovine serum albumin (BSA: Molecular weight of 66, 000 Da). This BSA rejection test was done to confirm the class of fabricated BHFMs are in the ultrafiltration range [41]. Chiam and Rosalam reported that the molecular weight range for testing ultrafiltration membranes is from 20, 000 Da to 500, 000 Da [42]. The molecule's radius of 66, 000 Da BSA can be calculated by Equation 5:

$$\boldsymbol{\alpha = 0.33M^{0.46}} \qquad \text{(Equation 5)}$$

where α represents the molecule radius (nm) and M represent the molecular weight (Da). According to this equation, the molecular radius of this 66,000 Da BSA is 54.4 nm. The molecular radius of BSA is within the ultrafiltration pores range (10 – 100 nm) and smaller than microfiltration pores range (100 – 1000 nm). Thus, BSA was used to evaluate the rejection rate of the fabricated membranes.

2 L of 1000 ppm BSA solution was loaded into the membrane module filtration apparatus and 10 cm of each BHFMs were assembled in the system. The rejection analysis was performed in a cross-flow mode through outside-in configuration. All the loaded membrane samples were tested from 0.5, 1.0, 1.5, 2.0, 3.0, 4.0, 5.0 and 6.0 bar trans-pressure, same as the permeability test. The membranes were rinsed with deionized water for 5 min after each circle of the filtration test. The rejection is defined using Equation 6:

$$\boldsymbol{R = \left(1 - \frac{C_p}{C_f}\right) x\ 100\%} \qquad \text{(Equation 6)}$$

where R is the BSA rejection rate (%), and C_p and C_f represent the concentrations of BSA in the permeate and feed solutions respectively. The determination of BSA content in influent and

effluent solutions were measured using UV-Vis spectrophotometer (DR5000, HACH) with absorption wavelength of 278 nm.

2.4.4 Membrane fouling studies

The deposition of foulant material in the bare BHFM and ZnO-incorporated BHFM were studied in this research work. Membrane fouling is an attachment process of foulant particles or impurities present in the treating wastewater in membrane structure. The attachment of the foulant can be on and in membrane's structure. The deposition of these fouling materials on the membrane surface can disrupt the membrane's performance in terms of its permeate flux and rejection rate. Antifouling performance of BHFM1 and BHFM4 in 1000 ppm BSA solution was investigated using cross-flow filtration system in laboratory setup at pressure 1.0 bar. The BHFMs were allowed to filter BSA solution for a complete one circle of filtration for a duration of 240 min and volume of flux (ml) was recorded at 30 min intervals to evaluate the fouling behavior. 10 ml of effluent solution was collected at 30 min intervals to evaluate the rejection rate. Upon completion of one cycle of filtration for 240 min, the membranes were detached from the filtration system and rinsed under running water for 30 min without applying any additional pressure on it. After the washing process of the membrane is completed, the membranes were once again subjected to the next cycle of filtration testing. A total of 3 cycles of the filtration process were conducted to evaluate the membrane reusability. Equation 7 was used to evaluate the flux recovery percentage;

$$\boldsymbol{FR = \frac{Fi}{Fw} \times 100} \qquad \text{(Equation 7)}$$

where, *FR* is the flux recovery percentage, *Fi* is initial flux of BSA solution in L/m^2h and *Fw* is the flux obtained after the membranes were rinsed for 30 min in L/m^2h.

2.4.5 Mechanical strength

The mechanical strengths of the braid support and best-performing BHFM were measured using tensile testing apparatus (AG-X Plus). Samples of length 150 mm with clamping distance of 100mm were placed vertically between a pair of pneumatic clamps and stretched at 20 mm/min at

upper clamp. The tensile stress of the samples were recorded at the maximum force on samples to break. Three specimens were tested to get the average tensile stress value.

3.0 Results and discussion

Figure 2 represents the XRD pattern recorded for the synthesized ZnO nanoparticles. The obtained nanoparticles are polycrystalline and the diffraction data agreed well with JCPDS card of ZnO nanoparticles (JCPDS 36-1451) with 2θ peaks at t 31.633 (1 0 0), 34.278 (0 0 2), 36.115 (1 0 1), 47.403 (1 0 2), 56.472 (1 1 0), 62.693 (1 0 3), 67.813 (1 1 2), 68.975° (2 0 1) and 72.42 (202). The pattern does not contain any other impurity peaks which proves the pure quality of the synthesized nanoparticles. This result pattern is corresponding to the results obtained by Borker and Desai [43]. They observed major diffraction peaks at 31.73, 34.39, 36.24, 47.51, 56.52, 62.88, 72.54 and 76.89 which assigned as (1 0 0), (0 0 2), (1 0 1), (1 0 2), (1 1 0), (1 0 3), (1 1 2), (2 0 1) and (2 0 2) planes respectively. The crystalline size of the nanoparticles were calculated using Hall-Williamson method [38]. The average crystallite size of the synthesized ZnO nanoparticles were 10 ± 1.8 nm.

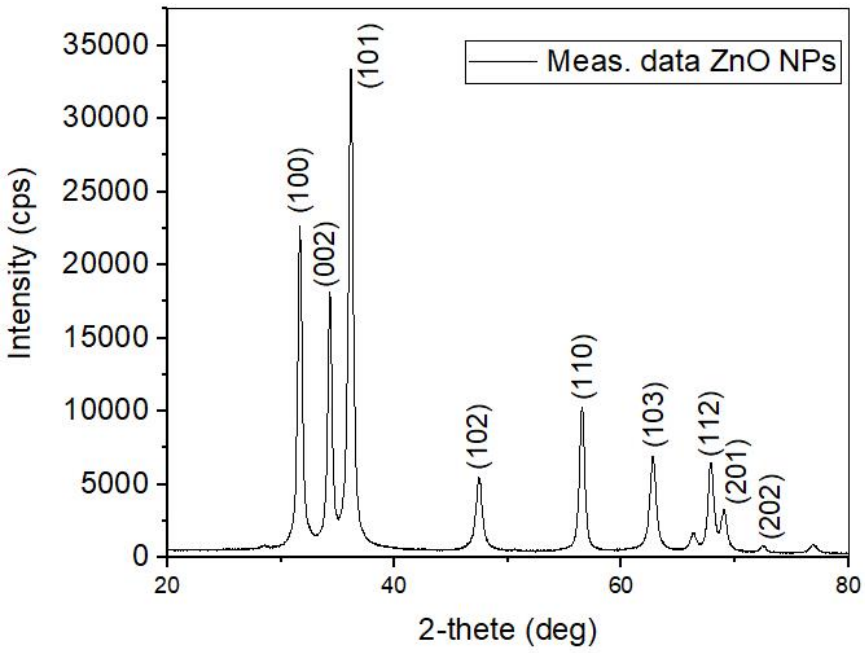

Figure 2 XRD pattern of ZnO nanoparticles calcinated at 400 °C for 3 h.

The morphological examination by SEM analysis in Figure 3 shows that the fabricated HFM membrane is highly porous compared to the BHFMs. Finger-like structures were observed in both HFM and BHFMs. Figure 3 (a) and (b) shows the morphology of a neat PSf HFM. The membrane exhibits well-defined structures, i.e. tiny finger-like at its selective outer layers, large and repetitive macro voids underneath the selective layer and well-distributed finger-like structures at bottom layer. Figure 3 (c) and (d) shows the morphology of the BHFM1. The membrane exhibits well-defined membrane structure, i.e., finger-like and micro voids at its outer selective layer, macro voids underneath selective layer, sponge structures underneath the macro voids and a small amount of the PSf coating solution which infiltrated into the braid support. This morphology is corresponding to the result shown by Zhou et al. [44]. Two skin layers were observed in the HFM, whereas in BHFMs only one skin layer was observed. Figure 3 (e)-(j) shows the PSf BHFM incorporated with different loadings of ZnO nanoparticles. The loading of the ZnO nanoparticles were increased to 0.5 wt.% (Figure 3 (e) and (f)), 1.0 wt.% (Figure 3 (f) and (g)) and 1.5 wt.% (Figure 3 (h) and (i)).

BHFM2 and BHFM3 exhibits wider finger-like structures with dense skin layer at its outer selective layers, macro voids and sponge structures underneath the selective layer and a small amount of PSf coating solution which infiltrated into the braid support. Meanwhile, BHFM4 exhibits macro finger-like structures and thin skin separating layer at its outer selective layer, macro voids underneath selective layer, thick sponge structures before the braid support and a small amount of PSf coating solution which infiltrated into the braid support. The macro voids and dense sponge structure observed near the braid support are responsible for higher permeation [45]. This was possibly due to the hydrophilic properties of the ZnO nanoparticles which makes the water move faster into the membrane compared to the de-mixing rate between solvent and non-solvent during the phase inversion process [26,45]. In this study the addition of ZnO nanoparticles in the dope solution were believed to delay the de-mixing process between solvent and non-solvent which increased the formation of macro voids. The incorporation of non-solvent material in the dope solution has increased the viscosity, and consequently the kinetic exchange mechanism of the solvent and water in the coagulation bath has become slower. Thus the macro voids structures are formed [46,47]. This mechanism is corresponding to reports by Fan et al., where they detailed that the formation of the macro void pores in the separation layers is due to the transition from

delayed de-mixing to instantaneous de-mixing which mainly happens on the addition of non-solvent materials in the dope solution [35].

From the morphology of the BHFMs, it can be clearly observed that the infiltration of the dope solution was promoted with the introduction of the ZnO nanoparticles. This is due to the hydrophilic property of the doping solution which can easily infiltrate the braid support and accumulate in-between the braid channels during the fabrication process [48]. This infiltration of small amounts of dope solution into braid supports as shown in Figure 4 (b) and (f) promotes a good interfacial bond between the separation layer and braid support. Cheng et al. reported that the intrusion of the dope solution into the braid support increased the mechanical stability of the braided membranes [32]. This is due to the separation layer being tightly bonded with the braids, preventing the delamination of the separation layer from the braid support. Table 4 illustrates the thickness of the separation layer, outer diameter and inner diameter of the fabricated HFM and BHFMs. From the measured thickness of BHFMs, it can be observed that BHFM1 has a thicker separation layer compared to the other BHFMs. Again, this is due to lower infiltration rate of PSf dope solution compared to ZnO/PSf dope solution. Moreover, different thicknesses of separation layer were observed in all BHFMs. This is also closely related to the infiltration rate of the dope solution into the braid support, and the uneven round shape of the braid support during the spinning process due to mechanical stress applied to pull the braid support out from spinneret system. These results correspond to the result obtained by Liu et al. [34]. They explained that this uneven separation layer thickness is due to the pulling force applied during the fabrication of BHFMs, which change the density of braid support and position or angle of the braid in spinneret. Therefore, the infiltration rate of the dope solution into the braid support is not uniform.

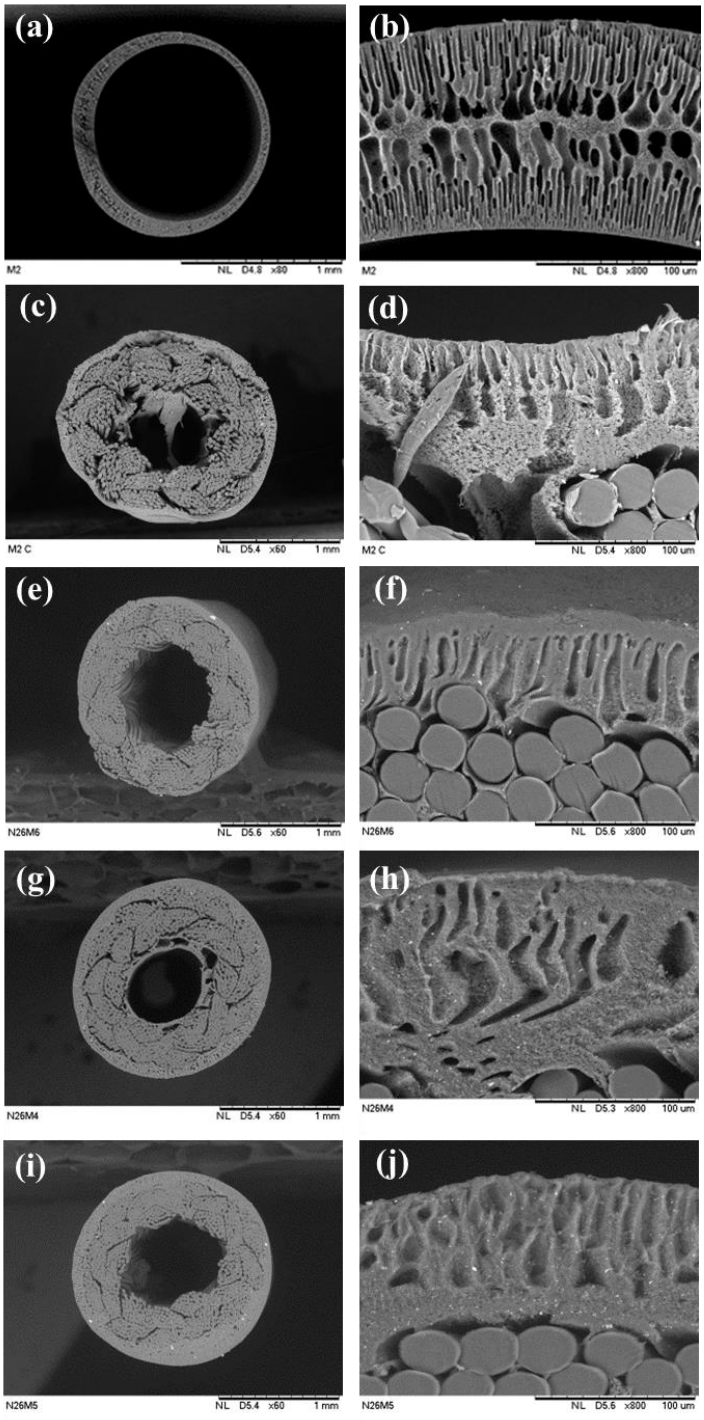

352

353 Figure 3 Morphology and separation layer of HFM and BHFMs: (a) cross-section
354 morphology of neat PSf HFM, (b) separation layer of neat PSf HFM, (c) cross-section
355 morphology of BHFM1, (d) separation layer of BHFM1, (e) cross-sectional morphology of
356 BHFM2, (f) separation layer of BHFM2, (g) cross-sectional morphology of BHFM3, (h) cross-
357 sectional morphology of BHFM4, (i) cross-sectional morphology of BHFM4 and (j) separation
358 layer of BHFM4.

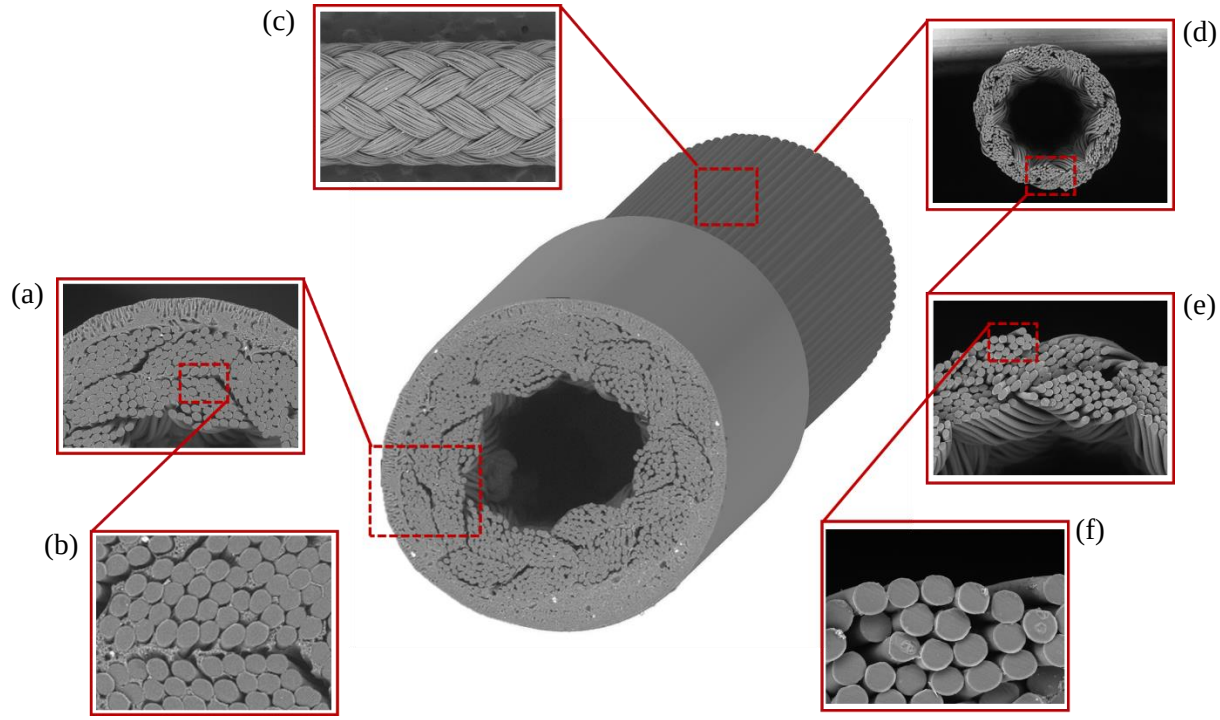

Figure 4 Typical BHFM structure diagram and morphology of typical separation layer, (a) typical morphology of BHFM, (b) adhesion of dope solution with braid support, (c) surface of braid support, (d) cross-sectional morphology of braid support, (e) cross-section of PET twisted fiber bundle morphology and (f) braid support arrangement before membrane fabrication.

Table 3 Thickness, outer and inner diameter of HFM and BHFM.

Membrane	Thickness (μm)	Thickness of braid support (μm)	Outer diameter (μm)	Inner diameter (μm)
HFM	96.66 ± 42.44	n.a.	1250.20 ± 22.70	1075.37 ± 26.17
BHFM1	89.82 ± 38.38	430.62 ± 35.20	1712.97 ± 78.97	672.10 ± 103.60
BHFM2	74.73 ± 28.17	290.74 ± 52.36	1576.33 ± 73.77	845.40 ± 89.80
BHFM3	81.96 ± 44.14	412.53 ± 28.68	1637.57 ± 51.07	648.60 ± 44.60
BHFM4	84.49 ± 23.81	372.14 ± 37.59	1639.17 ± 10.87	752.90 ± 92.50

The water contact angles of BHFM1, BHFM2, BHFM3 and BHFM4 are 108.79°, 83.54°, 77.04° and 71.02° respectively (Table 4). The presence of ZnO nanoparticles in PSf BHFM has improved its hydrophilicity by at least 37.77°, which can be explained as the large number of

oxidized functional groups on the surface of the membrane after modification, which has a positive effect on improving the hydrophilicity of the membranes [49]. The contact angle results correspond to the result shown by Pintilie et al. [50], where they reported that the presence of 1.0 wt.% of ZnO in PSf HFM improved the hydrophilicity by 23.50°. Balta et al. reported that 2.0 wt.% of ZnO nanoparticles in the PES membrane dropped the contact angle significantly from 70.00° to about 57.00°. This shows that the incorporation of the ZnO nanoparticles has significantly modified the membrane surface to be more hydrophilic.

Table 4 Water contact angle values for fabricated BHFM prepared in various ZnO nanoparticles concentration.

Membrane code	**BHFM1**	**BHFM2**	**BHFM3**	**BHFM4**
Average contact angle (°)	108.79	83.54	77.04	71.02
Standard error	± 3.207	± 1.535	± 3.209	± 0.926

The tensile stress of the braid support and best-performing membrane BHFM4 were measured, and the stress-strain data are plotted as shown in Figure 5. The braid support and BHFM4 exhibited super-high tensile stress at break 118.127MPa and 85.501MPa respectively. It can clearly be seen that the tensile strength and elongation at break of the BHFM membrane is less compared to the braid support. The lower mechanical strength of the BHFM is due to the alkaline pre-treatment of the braid support. The obtained tensile strength of both braid support and BHFM are corresponding with results reported by Zhou et al., Quan et al., and Liu et al., where they reported the tensile strength of braided membranes are from 80 MPa to 160 MPa [44,48,52–54]. The obtained tensile stress of BHFM is 4 times higher as compared self-supporting HFM which are typically from 2 MPa to 22 MPa [44,55,56]. The membrane mechanical strength is one of factors which is limiting its applications in wastewater treatment systems. Based on the tensile test result, the BHFMs could be an effective membrane in high-pressure wastewater treatment systems. Based on the other research's findings, the mechanical strength of the braided membranes is dependent on the mechanical strength of the selected braid support rather than the mechanical strength of the coating layers [1,48,52,54]. Along with this, we also can observe that the elongation of the braided membrane is lower than the braid support; which is 26.910% and 35.815% for BHFM4 and braid support respectively. This is due to the formed coating layer and infiltrated separation layers in the braid support limiting the deformation of the braid, and inhibiting the

straining of the braided membrane. Many research studies claims high tensile stress of braided membranes; however, they also placed their concern on the delamination of the coating layers which related to the poor interfacial bonding strength between separation layer and braid surface. The poor interfacial bonding between coating layer and braid support could restrict the lifetime of the membranes [36,44].

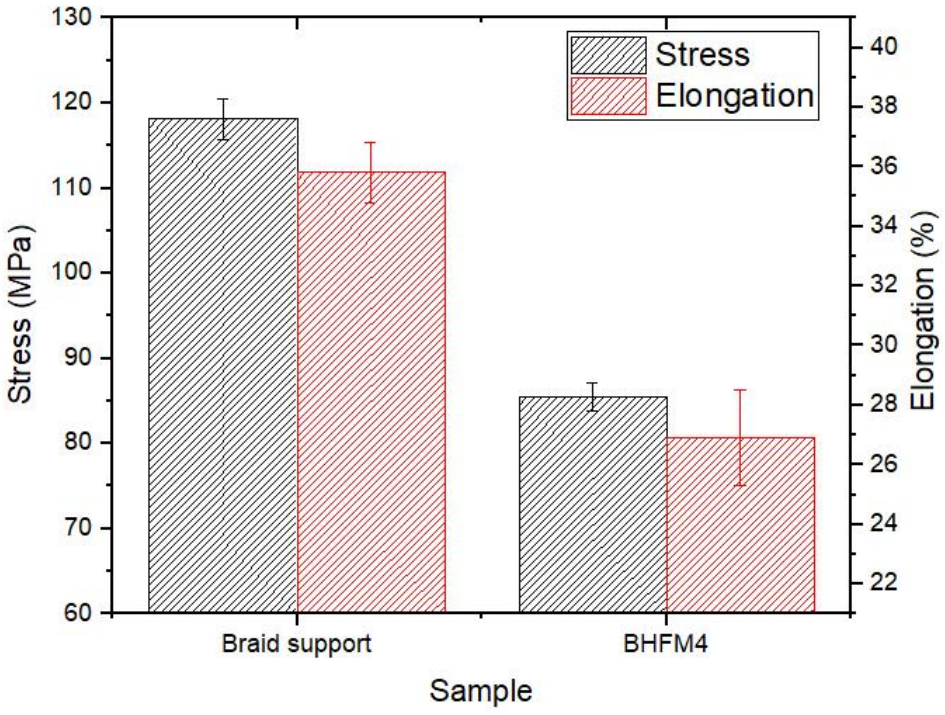

Figure 5 Stress-strain diagram of braid support and braided membrane.

The water flux and BSA rejection rate of neat PSf HFM and all BHFMs are depicted in Figure 6. Figure 6 shows that the BHFM4 has a higher flux of 919.12 L/m^{2}h and an average of 97.34 % BSA rejection rate compared to neat PSf HFM (with an average flux of 346.20 L/m^{2}h and BSA rejection of 49.20%) and other ZnO/PSf BHFMs at 1.0 bar pressure. The high flux of BHFM4 is due to the -OH of ZnO nanoparticles in the membrane separation layer which absorbs water molecules and the strong electronegativity of ZnO nanoparticles which has hindered the adsorption and deposition of BSA proteins in membrane separation layer.

The braid's fabric nature to absorb the filtrated water molecules as well as the porous structure of braid support also contributed to the high flux. Despite that, the reduced thickness of the membrane separation layer in BHFMs compared to self-supported HFMs (as shown in Table 3) also contributed to the increase in water flux. Overall, both the thin hydrophilic separation layer and the high water-attracting character of the braid support have played an important role in this high flux achievement.

Initially, at 0.5 and 1.0 bar, neat PSf HFM has shown slightly higher flux then the neat BHFM with 51.07 and 49.20% of BSA rejection rate. Later, the pure water flux observed at pressure $\geq$1.5 bar from neat PSf HFM was higher than BHFM1 and BHFM2. However, the BSA rejection rate was low. These show that the HFM is collapsed at pressure $\geq$ 1.5 bar. At the same moment, the neat PSf BHFM membrane has obtained flux until 6.0 bar with constant rejection rate. The intrusion of 0.5 wt.% ZnO nanoparticles in PSf BHFM has increased flux up to 2.9 times at pressure 6 bar with more than 91.96% of BSA rejection. BHFM3 has obtained its maximum flux 1860.40 L/m^{2}h at 5.0 bar with 96.28% BSA rejection rate and BHFM4 has obtained its maximum flux 1909.90 L/m^{2}h at 4.0 bar with 97.34% BSA rejection rate. This proves that the fabricated BHFMs are able to withstand higher pressures compared to HFMs. Pure water flux trend indicates that the addition of ZnO nanoparticles into the membrane mixed matrix has improved hydrophilicity and flux performance. This is due to the large quantity of -OH present on the ZnO nanoparticles which are contributing to the development of the hydrophilic property, which in turn improves the permeability. This enhanced hydrophilicity of the membrane improved the absorption capability of water molecules within the membrane matrix.

On the basis of BSA rejection, all BHFMs were able to remove more than 90% of BSA. This result indicates that the incorporation of ZnO nanoparticles gives better flux performance than BSA rejection. This result pattern is corresponding to the results obtained by Adilah et al. and Abdi et al. [45][51].

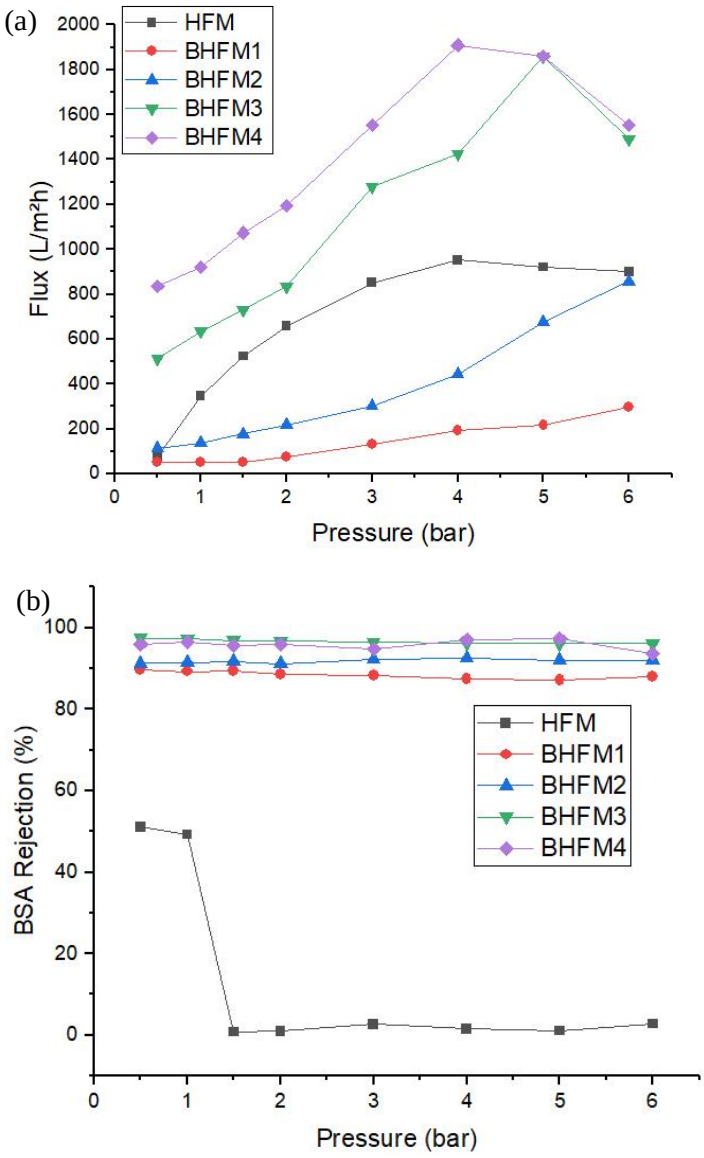

Figure 6 (a) Water flux permeation and (b) rejection in BSA.

Figure 7 shows the changes in BSA permeate flux over filtration cycles. Both BHFM1 and BHFM4 exhibit drops in flux over time and cycles. The attachment of BSA particles on the braided membranes as fouling materials over time is the reason behind to this reduction in flux. Both membranes have shown almost similar flux pattern throughout the three cycles. However, BHFM4 showed a lower flux drop of about *14.30%;* while BHFM1 showed major drops in flux of about 28.50% throughout the three circles. This indicates that BHFM1 experienced a higher fouling rate compared to BHFM4; which can be attributed to its low hydrophilic nature; which allows deposition of protein molecules on the membrane separation layer. The fouling phenomenon on

454 the membrane surface can be related with the strong interaction of separation particles in
455 wastewater with properties of membrane materials. Hence, the interaction of BSA particles with
456 hydrophilic ZnO/PSf BHFM is the most crucial part in the fouling behaviour study. In this study,
457 the strong electronegativity and excellent hydrophilicity of BHFM4 compared with BHFM1 has
458 hindered the irreversible adsorption and deposition of BSA proteins on the membrane separation
459 layer, which is also believed to improve the antifouling properties of membranes [32].

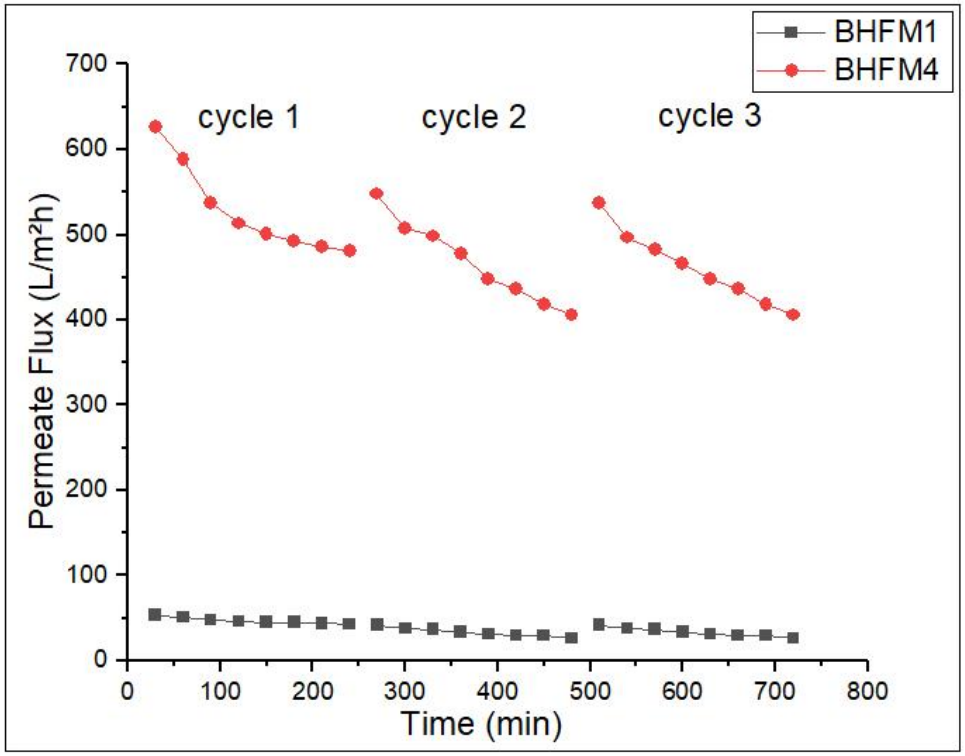

460

461 Figure 7 BSA flux for five circles of BSA filtration
462

463 Table 5 illustrates the flux and rejection performance of the incorporated additive in
464 braided/reinforced braided hollow fiber membranes as reported in the literature. BHFM4 has
465 reasonably high flux permeation rate compared to flux reported by other researchers at pressure
466 1.0 bar. Hao et al. reported that the incorporation of 0.5 wt % of GE improved the flux permeate
467 from 44.00 to 65.00 L/m^{2}h [57]. Similarly, Wu et al. reported incorporation of 0.3 wt.% of GE
468 were increased the flux performance of BHFM from 350.00 to 1443.00 L/m^{2}h [36]. They reported
469 the highest flux permeate with 99.0% of kerosene rejection. This shows that the incorporation of
470 nanomaterial is able to increase flux performance. Similarly in this study the incorporation of ZnO

nanoparticles in a BHFM mixed matrix has improved flux performance from 32.20 L/m^{2}h to 919.12 L/m^{2}h. From literature, all research works which carried out studies with polymer concentration more than 13.0 wt.% reported more than 90.00% rejection rate. A similar pattern of rejection rate was observed in this study. Additionally, the fabricated BHFMs were successfully operated up to 6.0 bar pressure and high flux with stable BSA rejection rate were obtained. These results have added value for the study of fabricating high flux BHFMs.

Table 5 Flux and rejection of BHFM4 with other braided/reinforced hollow fiber membrane from the published literature.

Membrane material	**Additive (wt.%)**	**Pressure (bar)**	**Impurities**	**Pure water flux (L/m^{2}h)**		**Rejection (%)**	**Ref**
				Neat BHFM	**Modified BHFM**		
13.0 wt.% PVDF	0.5 wt.% Graphene	1.0	kerosene and water mixture (1: 1, v/v)	44.0	65.0	99.7	[57]
11.5 wt.% PVC	11.5 wt. % poly(ethylene glycol) methyl ether methacrylate	0.5	100ppm latex particle solution	35.0	72.0	76.0	[44]
12.0 wt.% PVC	10.0 wt.% polyvinylpyrrolidone	1.0	1000ppm BSA solution	n.a.	700.0	71.0	[53]
20.0 wt.% PIP	1.0 wt.% trimesoyl chloride	1.0	2000ppm NaCl and 2000ppm $MgSO_4$ solution	17.0	23.0	30.0 65.0	[58]
16.0 wt.% PU	0.3 wt.% Graphene	1.0	kerosene and water mixture (1: 1, v/v)	350.0	1443.0	99.0	[36]
13.0 wt.% PVC	4.0 wt.% Silicon dioxide	1.0	kerosene and water mixture	30.0	50.0	98.0	[59]
16.0 wt.% PSf	1.5 wt.% ZnO	1.0	1000ppm BSA solution: 54.4nm particle size	36.2	919.1	96.5	This work

4.0 Conclusion

In summary, the BHFM incorporated with different loadings of ZnO nanoparticles has successfully been fabricated via dry-wet phase inversion technique. The fabricated membrane possessed good morphology with finger-like voids on the outer separation layer, sponge-like structure and good adhesion with braid support. When the ZnO nanoparticles content reached 1.5 wt.%, the morphology of BHFM had good infiltration rate of dope solution into the braid support due to the hydrophilic nature of the ZnO/PSf doping solution, which also promoted a good interfacial bond between the separation layer and braid support. The infiltration rate of dope solution has developed different thicknesses of separation layers in all BHFMs. The incorporation of 1.5 wt.% of ZnO nanoparticles in PSf BHFM membrane also increased the hydrophilic properties of the BHFM from 108.79° to 71.021°. High water permeability and an excellent BSA rejection rate (97.1%) were achieved at 1.5 wt.% of ZnO nanoparticles compared to 0.0, 0.5, 1.0 wt.% BHFMs. Good fouling stability and recovery after three cycles of BSA filtration were observed. The results show that the BHFM exhibit high mechanical strength and remarkable elongation which makes this membrane have a high potential application prospect in wastewater treatments.

Altogether, the hybrid ZnO /PSf BHFM exhibits superior hydrophilicity and higher permeability compared with neat PSf BHFM and PSf HFM. Additionally, it was also observed that the BHFMs are able operate at higher pressures up to 4.0 bar easily with >90% rejection rate, compared to HFM which collapsed at 1.5 bar pressure in this research work. 1.5 wt.% ZnO nanoparticle in 16 wt.% PSf BHFM appears to be the most promising range in improvising hydrophilicity and permeability.

CRediT authorship contribution statement

Prakash Peechmani: Writing - original draft, Conceptualization, Methodology, Validation, Formal analysis, Investigation, Data curation. **Mohd Hafiz Dzarfan Othman**: Conceptualization, Methodology, Validation, Formal analysis, Investigation, Resources, Writing - review & editing, Supervision, Project administration, Funding acquisition. **Roziana Kamaludin**: Validation, Resources, Writing - review & editing, Supervision. **Mohd Hafiz Puteh**: Validation, Resources,

Writing - review & editing, Supervision. **Juhana Jaafar**: Validation, Formal analysis, Investigation, Writing - review & editing. **Mukhlis A Rahman**: Validation, Formal analysis, Investigation, Writing - review & editing. **Ahmad Fauzi Ismail**: Validation, Resources, Writing - review & editing, Project administration, Funding acquisition. **Siti Hamimah Sheikh Abdul Kadir**: Validation, Writing - review & editing. **Rosli Md. Illias**: Validation, Writing - review & editing. **Joe Gallagher**: Validation, Writing - review & editing. **Sabreenna Marsya Djuli**: Validation, Writing - review & editing.

Acknowledgement

The authors gratefully acknowledge financial support from the Ministry of Higher Education Malaysia under the Higher Institution Centre of Excellence Scheme (Project Number: R.J090301.7809.4J430) and Universiti Teknologi Malaysia under the Collaborative Research Grant (Project number: R.J130000.7351.4B418), Award Grant (Project number: R.J130000.7709.5M003) and International and Industry Incentive Grant (IIIG) (Project number: Q.J130000.3009.02M25). The authors would also like to thank Research Management Centre, Universiti Teknologi Malaysia for the technical support.

Reference

[1] L. Liu, H. Shen, T. Li, Y. Han, Interface treatment and performance study on fiber tube reinforced polyvinylidene fluoride hollow fiber membranes, J. Text. Inst. 111 (2020) 1054–1063.

[2] X. Zhang, Y. Guo, T. Wang, Z. Wu, Z. Wang, Antibiofouling performance and mechanisms of a modified polyvinylidene fluoride membrane in an MBR for wastewater treatment: Role of silver@silica nanopollens, Water Res. 176 (2020) 115749.

[3] K. Xiao, S. Liang, X. Wang, C. Chen, X. Huang, Current state and challenges of full-scale membrane bioreactor applications: A critical review, Bioresour. Technol. 271 (2019) 473–481.

[4] S. Rezaei Soulegani, Z. Sherafat, M. Rasouli, Morphology, physical, and mechanical

properties of potentially applicable coelectrospun polysulfone/chitosan-polyvinyl alcohol fibrous membranes in water purification, J. Appl. Polym. Sci. 138 (2021) 1–12.

[5] L. Zhu, H. Song, G. Wang, Z. Zeng, Q. Xue, Symmetrical polysulfone / poly (acrylic acid) porous membranes with uniform wormlike morphology and pH responsibility : Preparation , characterization and application in water puri fi cation, J. Memb. Sci. 549 (2018) 515–522.

[6] Z. Harun, M.Z. Yunos, K.N. Yusof, M.F. Shohur, W.J. Lau, W.N.W. Salleh, Optimization and characterization of polysulfone membranes made of zinc oxide, polyethylene glycol and eugenol as additives, J. Eng. Sci. Technol. 11 (2016) 1001–1015.

[7] L. Zhu, M. Wu, B. Van Der Bruggen, L. Lei, L. Zhu, Separation and Purification Technology Effect of TiO_2 content on the properties of polysulfone nano filtration membranes modified with a layer of TiO_2 – graphene oxide, 242 (2020).

[8] R. Singh, M. Kumar, M. Kumar, Separation and Purification Technology Stimuli responsive mixed matrix polysulfone ultrafiltration membrane for humic acid and photocatalytic dye removal applications, Sep. Purif. Technol. 250 (2020) 117247.

[9] M.S. Fahmey, A.H.M. El-Aassar, M. M.Abo-Elfadel, A.S. Orabi, R. Das, Comparative performance evaluations of nanomaterials mixed polysulfone: A scale-up approach through vacuum enhanced direct contact membrane distillation for water desalination, Desalination. 451 (2019) 111–116.

[10] I. Gede Wenten, Y.S. Syaifi, F.A. Saputra, M. Zunita, H. Julian, K. Khoiruddin, P.T.P. Aryanti, Preparation of antibacterial and antifouling PSF/ZnO/ eugenol membrane for peat water ultrafiltration, Water Sci. Technol. Water Supply. 19 (2019) 2248–2255.

[11] P. Mondal, N.S. Samanta, A. Kumar, M.K. Purkait, Recovery of H 2 SO 4 from wastewater in the presence of NaCl and $KHCO_3$ through pH responsive polysulfone membrane : Optimization approach, Polym. Test. 86 (2020) 106463.

[12] L.M. Robeson, A. Noshay, M. Matzner, C.N. Merriam, Physical Property Characteristics, Die Angew. Makromol. Chemie. 30 (1973) 47–62.

[13] I. Cabasso, E. Klein, J.K. Smith, Polysulfone hollow fibers. Spinning and properties, J.

Appl. Polym. Sci. 20 (1976) 2377–2394.

[14] S.S.M. Lock, K.K. Lau, N. Jusoh, A.M. Shariff, Y.F. Yeong, C.L. Yiin, S.A. Ammar Taqvi, Physical property and gas transport studies of ultrathin polysulfone membrane from 298.15 to 328.15 K and 2 to 50 bar: atomistic molecular simulation and empirical modelling, RSC Adv. 10 (2020) 32370–32392.

[15] H. Jiang, T. Wang, S. Li, Z.P. Zhao, Fabrication of porous polymer membrane from polysulfone grafted with acid ionic liquid and the catalytic property for inulin hydrolysis, J. Memb. Sci. 618 (2021) 118742.

[16] J.H. Jhaveri, Z.V.P. Murthy, A comprehensive review on anti-fouling nanocomposite membranes for pressure driven membrane separation processes, Desalination. 379 (2016) 137–154.

[17] H. Borji, G.M. Ayoub, N. Nassar, L. Malaeb, How effective are nanomaterials for the removal of heavy metals from water and wastewater ?, (2020).

[18] P. Dong, J. Feng, D. Zhang, C. Li, Q. shan Shi, X. Xie, In situ synthesis of amply antimicrobial silver nanoparticle (AgNP) by polyzwitterionic copolymers bearing hydroxyl groups, React. Funct. Polym. 153 (2020) 104609.

[19] M.J. Sydor, D.S. Anderson, H.B.B. Steele, J.B.A. Ross, BBA - Biomembranes Effects of titanium dioxide and zinc oxide nano-materials on lipid order in model membranes, BBA - Biomembr. 1862 (2020) 183313. https://doi.org/10.1016/j.bbamem.2020.183313.

[20] R. Rajakumaran, M. Kumar, R. Chetty, Morphological effect of ZnO nanostructures on desalination performance and antibacterial activity of thin-film nanocomposite (TFN) membrane, Desalination. 495 (2020) 114673.

[21] T. Munawar, F. Mukhtar, M. Shahid, M. Riaz, M. Naveed, K. Mahmood, M. Hasan, M.I. Arshad, F. Hussain, A. Hussain, F. Iqbal, Novel photocatalyst and antibacterial agent ; direct dual Z-scheme ZnO – CeO_2 -Yb_2O_3 heterostructured nanocomposite, Solid State Sci. 109 (2020) 106446.

[22] F. Kazemi, Y. Jafarzadeh, S. Masoumi, M. Rostamizadeh, Oil-in-water emulsion separation by PVC membranes embedded with GO-ZnO nanoparticles, J. Environ. Chem.

595 Eng. 9 (2021) 104992.

596 [23] S. Abdi, M. Nasiri, S. Yuan, J. Zhu, B. Van der Bruggen, Fabrication of PES-based super-
597 hydrophilic ultrafiltration membranes by combining hydrous ferric oxide particles and UV
598 irradiation, Sep. Purif. Technol. 259 (2021) 118132.

599 [24] J. Xiong, Y. Gong, C. Ma, X. Zuo, J. He, Fabrication and characterization of
600 polyvinylidene fluoride/zinc oxide membranes with antibacterial property, J. Water
601 Supply Res. Technol. 69 (2020) 122–133. https://doi.org/10.2166/aqua.2019.004.

602 [25] M. Amini, M. Seifi, A. Akbari, M. Hosseinifard, Polyamide-zinc oxide-based thin film
603 nanocomposite membranes: Towards improved performance for forward osmosis,
604 Polyhedron. 179 (2020) 114362.

605 [26] T.D. Kusworo, W. Widayat, D.P. Utomo, Y.H.S. Pratama, R.A.V. Arianti, Performance
606 evaluation of modified nanohybrid membrane polyethersulfone-nano ZnO (PES-nano
607 ZnO) using three combination effect of PVP, irradiation of ultraviolet and thermal for
608 biodiesel purification, Renew. Energy. 148 (2020) 935–945.

609 [27] F. Sokhandan, M. Homayoonfal, F. Davar, Application of zinc oxide and sodium alginate
610 for biofouling mitigation in a membrane bioreactor treating urban wastewater, Biofouling.
611 0 (2020) 1–19.

612 [28] Z. Fan, C. Xiao, H. Liu, Q. Huang, J. Zhao, Structure design and performance study on
613 braid-reinforced cellulose acetate hollow fiber membranes, J. Memb. Sci. 486 (2015) 248–
614 256.

615 [29] K.C. Ueng, S.P. Wen, C.W. Lou, J.H. Lin, Braiding structure stability and section
616 treatment evaluations of braided coronary stents made of stainless steel and bio-
617 absorbable polyvinyl alcohol via a braiding technique, Fibers Polym. 16 (2015) 675–684.

618 [30] J. Yang, D. Sun, N. Hu, H. Ning, J. Zhang, W. Ye, J. Wu, Multi-objective robust design
619 optimization of a two-dimensional tri-axial braided hollow pillar using an evolutionary
620 algorithm, Compos. Struct. 220 (2019) 105–113.

621 [31] J. Yang, D. Sun, N. Hu, H. Ning, J. Zhang, W. Ye, J. Wu, Multi-objective robust design
622 optimization of a two-dimensional tri-axial braided hollow pillar using an evolutionary

623 algorithm, Compos. Struct. 220 (2019) 105–113.

624 [32] M. Chen, C. Xiao, C. Wang, H. Liu, Study on the structural design and performance of
625 novel braid-reinforced and thermostable poly(m-phenylene isophthalamide) hollow fiber
626 membranes, RSC Adv. 7 (2017) 20327–20335.

627 [33] R. Sengur-Tasdemir, B. Sayinli, G.M. Urper, H.E. Tutuncu, N. Gul-Karaguler, E. Ates-
628 Genceli, V. V. Tarabara, I. Koyuncu, Hollow fiber nanofiltration membranes with
629 integrated aquaporin Z, New J. Chem. 42 (2018) 17769–17778.

630 [34] K. Chen, C. Xiao, H. Liu, H. Ling, Z. Chu, Z. Hu, Design of robust twisted fiber bundle-
631 reinforced cellulose triacetate hollow fiber reverse osmosis membrane with thin separation
632 layer for seawater desalination, J. Memb. Sci. 578 (2019) 1–9.

633 [35] Z. Fan, C. Xiao, H. Liu, Q. Huang, Preparation and performance of homogeneous braid
634 reinforced cellulose acetate hollow fiber membranes, Cellulose. 22 (2015) 695–707.

635 [36] Y.J. Wu, C.F. Xiao, J. Zhao, Preparation of an electrospun tubular PU/GE nanofiber
636 membrane for high flux oil/water separation, RSC Adv. 9 (2019) 33722–33732.

637 [37] Y. Tao, M.M. Ba-abbad, A. Wahab, N. Hanis, H. Hairom, A. Benamor, Synthesis of
638 minimal-size ZnO nanoparticles through sol – gel method : Taguchi design optimisation,
639 JMADE. 87 (2015) 780–787.

640 [38] E.N. Danial, M. Hjiri, M.S. Abdel-wahab, N.H. Alonizan, L. El Mir, Antibacterial activity
641 of In-doped ZnO nanoparticles, Inorg. Chem. Commun. 122 (2020) 108281.

642 [39] T. Turken, R. Sengur-Tasdemir, E. Ates-Genceli, V. V. Tarabara, I. Koyuncu, Progress on
643 reinforced braided hollow fiber membranes in separation technologies: A review, J. Water
644 Process Eng. 32 (2019) 100938.

645 [40] J.H. Lee, S.H. Park, K.W. Oh, C.H. Lee, S.H. Kim, Effect of pretreatment conditions on
646 the hydrolysis and water absorption behavior of poly(ethylene terephthalate) fibrous
647 assembly, Polym. Int. 61 (2012) 657–663.

648 [41] M.N. Subramaniam, P.S. Goh, W.J. Lau, Y.H. Tan, B.C. Ng, A.F. Ismail, Hydrophilic
649 hollow fiber PVDF ultrafiltration membrane incorporated with titanate nanotubes for

650 decolourization of aerobically-treated palm oil mill effluent, Chem. Eng. J. 316 (2017)
651 101–110.

652 [42] C.K. Chiam, R. Sarbatly, Purification of aquacultural water: Conventional and new
653 membrane-based techniques, Sep. Purif. Rev. 40 (2011) 126–160.

654 [43] P. Borker, R. Desai, Enhanced photocatalytic activity of ZnO supported on Alumina and
655 Antibacterial study, Surfaces and Interfaces. 19 (2020) 100477.

656 [44] Z. Zhou, S. Rajabzadeh, L. Fang, T. Miyoshi, Y. Kakihana, H. Matsuyama, Preparation of
657 robust braid-reinforced poly(vinyl chloride) ultrafiltration hollow fiber membrane with
658 antifouling surface and application to filtration of activated sludge solution, Mater. Sci.
659 Eng. C. 77 (2017) 662–671.

660 [45] N. Adilah Rosnan, T.Y. Haan, A.W. Mohammad, The effect of ZnO loading for the
661 enhancement of PSF/ZnO-GO mixed matrix membrane performance, Sains Malaysiana.
662 47 (2018) 2035–2045.

663 [46] L. Jiang, J. Yun, Y. Wang, H. Yang, Z. Xu, Z. liang Xu, High-flux, anti-fouling dendrimer
664 grafted PAN membrane: Fabrication, performance and mechanisms, J. Memb. Sci. 596
665 (2020) 117743.

666 [47] H. Zhao, L. Wu, Z. Zhou, L. Zhang, H. Chen, Improving the antifouling property of
667 polysulfone ultrafiltration membrane by incorporation of isocyanate-treated graphene
668 oxide, Phys. Chem. Chem. Phys. 15 (2013) 9084–9092.

669 [48] Z. Zhou, L.F. Fang, S.Y. Wang, H. Matsuyama, Improving bonding strength between a
670 hydrophilic coating layer and poly(ethylene terephthalate) braid for preparing
671 mechanically stable braid-reinforced hollow fiber membranes, J. Appl. Polym. Sci. 135
672 (2018) 1–8.

673 [49] X.-T. Yuan, C.-X. Xu, H.-Z. Geng, Q. Ji, L. Wang, B. He, Y. Jiang, J. Kong, J. Li,
674 Multifunctional PVDF/CNT/GO Mixed Matrix Membranes for Ultrafiltration and Fouling
675 Detection, J. Hazard. Mater. 384 (2019) 120978.

676 [50] S.C. Pintilie, L.G. Tiron, A.L. Lazar, M. Vlad, I.G. Birsan, S. Balta, The influence of
677 ZnO/TiO_2 nanohybrid blending on the ultrafiltration polysulfone membranes, Mater. Plast.

55 (2018) 54–62.

[51] S. Abdi, M. Nasiri, S. Yuan, J. Zhu, B. Van der Bruggen, Fabrication of PES-based super-hydrophilic ultrafiltration membranes by combining hydrous ferric oxide particles and UV irradiation, Sep. Purif. Technol. 259 (2021) 118132.

[52] Q. Quan, C.F. Xiao, H.L. Liu, W. Zhao, X.Y. Hu, G.L. Huan, Preparation and properties of two-dimensional braid heterogeneous-reinforced polyvinylidene fluoride hollow fiber membrane, Adv. Mater. Res. 936 (2014) 218–225.

[53] H. Liu, S. Wang, J. Mao, C. Xiao, Q. Huang, Preparation and performance of braid-reinforced poly(vinyl chloride) hollow fiber membranes, J. Appl. Polym. Sci. 134 (2017) 1–10.

[54] Q. Quan, C. Xiao, H. Liu, Q. Huang, W. Zhao, X. Hu, G. Huan, Preparation and characterization of braided tube reinforced polyacrylonitrile hollow fiber membranes, J. Appl. Polym. Sci. 132 (2015) 1–10.

[55] C.Y. Lai, A. Groth, S. Gray, M. Duke, Preparation and characterization of poly(vinylidene fluoride)/nanoclay nanocomposite flat sheet membranes for abrasion resistance, Water Res. 57 (2014) 56–66.

[56] H.M. Mousa, H. Alfadhel, E.A. Nasr, Engineering and characterization of antibacterial coaxial nanofiber membranes for oil/water separation, Polymers (Basel). 12 (2020) 1–16.

[57] J. Hao, C. Xiao, T. Zhang, J. Zhao, Z. Fan, L. Chen, Preparation and Performance of PET-Braid-Reinforced Poly(vinylidene fluoride)/Graphene Hollow-Fiber Membranes, Ind. Eng. Chem. Res. 55 (2016) 2174–2182.

[58] L. Xia, J. Ren, J.R. McCutcheon, Braid-reinforced thin film composite hollow fiber nanofiltration membranes, J. Memb. Sci. 585 (2019) 109–114.

[59] H. Xu, H. Liu, Y. Huang, C. Xiao, Three-dimensional structure design of tubular polyvinyl chloride hybrid nanofiber membranes for water-in-oil emulsion separation, J. Memb. Sci. 620 (2021) 118905.